Optofluidic Intracavity Spectroscopy of Canine Lymphoma and Lymphocytes

Hua Shao, *Student Member, IEEE*, Weina Wang, *Student Member, IEEE*, Susan E. Lana, and Kevin L. Lear, *Member, IEEE*

***Abstract*—Multiple transverse mode, intracavity spectra of canine lymphoma cells in a passive Fabry–Pérot cavity are distinct from single-mode spectra of normal lymphocytes. Two-dimensional effective-index modal calculations provide insight into the nuclear size versus refractive index relationship and clarify the impact of lateral optical confinement on modal shift.**

***Index Terms*—Biophotonics, effective index model, optical cancer diagnostics, optofluidic intracavity spectroscopy.**

I. Introduction

LOW-COST and label-free identification of single biological cells is of broad interest in a variety of fields, including clinical diagnostics, drug delivery, food safety, and healthcare. The effective refractive index (RI) of a cell is a function of its size, shape, and intracellular components and can be used to measure its biological state [1]. For example, an enlarged nucleus has been used as an indication for precancer in clinical diagnosis [2]. Conventional microscopic imaging requires the use of stains to enhance contrast of the chromatin. Another traditional tool, flow cytometry, relies either on fluorescent labeling reagents or angle resolved scattering to differentiate cells but with nuclear size resolution of approximately 3% [3] although the variance in commercial instruments often limits their resolution to $\sim$1 μm [4]. Lab-on-a-chip methods offer the potential for application-specific tradeoffs in terms of cost, size, automation, and throughput relative to such established approaches. Biological cells inside an optical resonator modify the cavity modes, providing a probe for optical properties of the cells and their nuclei that can be used for cell recognition. Vertical external cavity surface-emitting-laser-based biosensors [5] were previously investigated. However, the fabrication of such active optical resonator-based sensors is challenging, requiring high gain to overcome the loss induced by the cell in order to reach threshold. We subsequently demonstrated a simple passive Fabry–Pérot (FP) cavity coated with gold mirrors for differentiating human blood cells [6]. A fiber-optic on-chip passive FP cavity [7] was also reported by researchers at Nanyang University, who measured the effective indexes and sizes of cancerous cells by differential longitudinal mode shift, although their analysis neglected multimode operation induced by the cells.

Manuscript received July 16, 2007; revised December 13, 2007.

H. Shao, W. Wang, and K. L. Lear are with the Electrical and Computer Engineering Department, Colorado State University, Fort Collins, CO 80523 USA (e-mail: Kevin.Lear@ColoState.edu).

S. E. Lana is with the Animal Cancer Center, Colorado State University, Fort Collins, CO 80523 USA.

Color versions of one or more of the figures in this letter are available online at http://ieeexplore.ieee.org.

Digital Object Identifier 10.1109/LPT.2008.918252

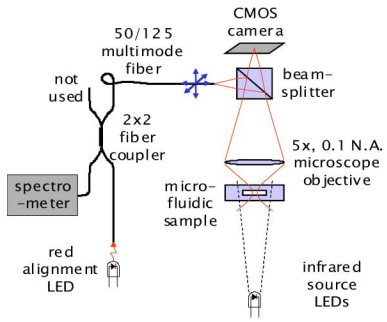

Fig. 1. Apparatus for single-cell optofluidic intracavity spectroscopy.

This letter focuses on investigating the lateral optical confinement of cancerous cells within passive microfluidic FP cavities. The phenomena of transverse modes giving rise to spectral content is similar to that reported by Gourley *et al.* [8] except there is no gain medium in passive cavities. An effective index model has been developed to explain the multimode spectra of cancerous cells and explore the nuclear size versus RI relationship.

II. Experimental Setup

Transmission spectra of single cells in an FP cavity filled with phosphate-buffered saline (PBS) solution were obtained using illumination from a near-infrared light-emitting diode (LED) (Hamamatsu L2690-02) with the apparatus illustrated in Fig. 1. Imaging of a multimode fiber onto the microfluidic channel served to spatially filter the transmitted light and select spectra either of individual cells or of the bare cavity for reference by changing the lateral position of the fiber. The 16-μm-deep interferometric cavity with a finesse $>$40 used in this study was similar to ones previously described [9] except that more robust HfO_2–SiO_2 dielectric mirrors with 13 quarter-wave layers, designed for 96% reflectivity in water at the LED peak wavelength of 890 nm, were used instead of gold mirrors. Fluids were delivered to the chip by pressure driven flow through nanoport assemblies (Upchurch Scientific N-124H).

III. Optical Spectroscopy

Transmission spectra of ten cancerous cells from each of two canine lymphoma cell lines as well as ten healthy lymphocytes centrifuged from peripheral blood mononuclear cells (PBMCs) were collected. A typical spectrum of lymphoma is shown in Fig. 2(a) together with bare cavity spectra taken at four different positions adjacent to the cell. Alignment of the four bare cavity spectra demonstrates the good cavity uniformity in the neighborhood of each cell although the bare cavity resonant wavelength does vary along the length of the channel. Transverse

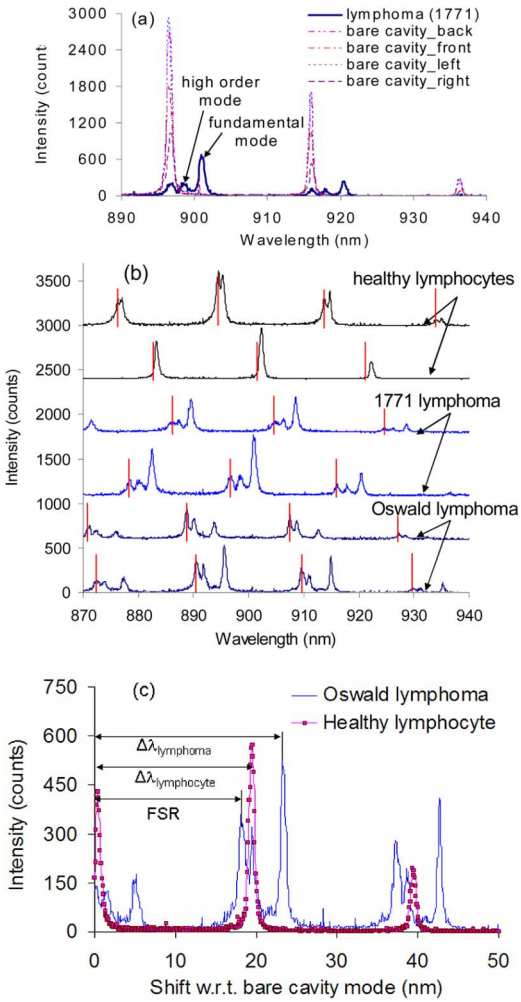

Fig. 2. Typical optofluidic intracavity transmission spectra of (a) 1771 canine lymphoma together with bare cavity spectra taken near the cell, (b) healthy canine lymphocytes and cancerous lymphoma cells from two different cell lines, Oswald and 1771, and (c) transverse mode shift for an individual lymphocyte from canine PBMCs and lymphoma.

mode groups are repeated for each longitudinal mode and are spaced by the cavity's free-spectral range (FSR) of ~20 nm. A cavity length of ~15.8 μm after thermal bonding was measured using $L_{\rm cav} = \lambda^2/(2n_0\Delta\lambda)$, where n_0 is the RI of PBS (phosphate 50 mM, NaCl 0.9%) and was determined to be 1.333, consistent with other reports [10], from $n_0 = n_{\rm DI}(\lambda/\lambda_{\rm DI})$ by measuring longitudinal mode shift of an FP cavity filled with DI water ($n_{\rm DI} = 1.330$) and then PBS. Fig. 2(a) clearly shows that the peaks near 896 and 916 nm in the lymphoma spectrum correspond to the residual transmission through the bare cavity around the cell. The other two modes in each transverse mode group, for example at 899 and 901 nm, are due to a combination of longitudinal mode shift and lateral confinement by the cell as will be discussed in detail below.

The longer wavelength (e.g., 901 nm) fundamental mode is dominated by the nucleus while the shorter wavelength (e.g., 899 nm) higher order mode has a higher overlap with the cytoplasm. Tighter focus of the light collection spot in the center of the cell increases the relative intensity of the longer wavelength mode. Fig. 2(b) shows representative spectra of individual lymphoma from two cell lines, labeled as "Oswald" and "1771"

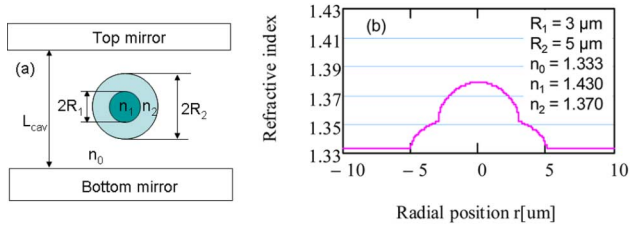

Fig. 3. (a) Illustration of the concentric spherical cell model in a microfluidic FP cavity. (b) Calculated effective RI profile of a concentric sphere loaded optofluidic microcavity.

together with spectra of healthy lymphocytes. The number of modes and spectral mode spacing for both the lymphocytes and the lymphoma cell lines were very repeatable except that the absolute wavelength of each mode group is shifted due to slight variations in the cavity length $L_{\rm cav}$ at different locations along the channel. The bare cavity wavelengths adjacent to each cell are indicated with vertical lines. While calculations described below indicate the existence of multiple transverse mode resonances for both healthy lymphocytes and lymphoma, higher order modes were experimentally observed only for lymphoma perhaps because the smaller nuclei of healthy lymphocytes result in weak lateral confinement.

In order to determine effective RIs for each cell mode relative to the bare cavity, an ambiguity in the absolute mode shift needs to be resolved. For example, lymphocytes exhibited only a single-mode red-shifted from the bare cavity by $\Delta\lambda = (j\ \mathrm{FSR} + 0.49) \pm 0.30$ nm, where j is the longitudinal mode order and $\mathrm{FSR} = 19.69$ nm. The corresponding effective RI is $n_{\rm lymphocyte} = 1.3345$, 1.3733, and 1.4105 for values of $j = 0, 1$, and 2, respectively. The range of previously reported lymphocyte RI [10], [11] suggests that $j = 1$ for this case. Thus, while the spectrum in Fig. 2(c) may appear to indicate only a very small $\Delta\lambda = 0.49$ nm, reasonable lymphocyte RI values require that lymphocytes shift the resonant wavelength from that of the bare cavity by $\Delta\lambda = 20.18 \pm 0.30$ nm or slightly more than one FSR.

The Oswald lymphoma cell line displayed a whole cell mode shift of 20.36 ± 0.40 nm corresponding to an effective index of 1.3737 ± 0.0008, and a nuclear mode shift of 24.59 ± 0.13 nm corresponding to an effective index of 1.3817 ± 0.0002. And the 1771 lymphoma cell line displayed a whole cell mode shift of 21.14 ± 0.23 nm and a nuclear mode shift of 23.61 ± 0.10 nm. Modeling of the cells allows the measured mode effective indexes to be used to extract material RIs for the cell cytoplasm and nucleus.

IV. Optical Modeling

The wavelength shift of cell modes from the bare cavity mode is related to the RIs and sizes of cellular features. A concentric double homogeneous RI sphere model, widely used in scattering spectroscopy [12], [13] and illustrated in Fig. 3(a), was employed in order to quantitatively analyze the spectra and extract RI information of the cells. Fig. 3(b) shows the effective RI profile of a double sphere loaded cavity in cylindrical coordinates obtained using an effective index model where the radial dependence of the RI was calculated from the cavity's

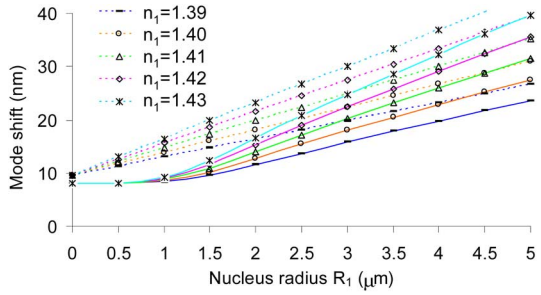

Fig. 4. Fundamental mode shift versus nucleus size and RI calculated with (solid lines) and without (dashed lines) lateral confinement using $n_{\text{effective}} = n(r = 0)$.

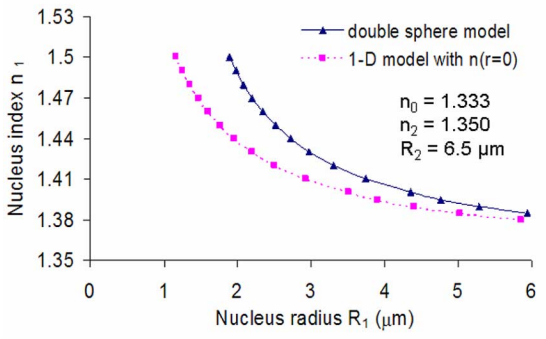

Fig. 5. Nuclear index versus radius by fitting the experimental spectrum of nuclear mode shift with the double-sphere model and the 1-D model.

resonant wavelength using the RI distribution to determine the effective path length at each radius [14] while neglecting reflections at the water-cytoplasm and cytoplasm-nucleus interfaces and treating the quarter-wave mirror stacks as 96% reflectors at single planes.

In the optical model, the cell radius was taken as $R_2 = 6.5$ μm based on microscopic measurements. The nuclear RI, $n_1 = 1.3987$, was first calculated using a double sphere model with $n_2 = 1.3550$ [11] and $R_1 = 3.5$ μm since the nuclear-to-cytoplasm volume ratio is approximately $1:5$ for normal cells [15]. Once the nuclear material RI was determined, the nuclear size of the cancerous lymphoma, $R_1 = 4.457$ μm, was calculated from the wavelength shift of 24.59 nm. The effects of nuclear size and RI on the mode shift are illustrated in Fig. 4 by computing the mode shift relative to the bare cavity mode, $\lambda_{\text{BC}} = 2n_0L_{\text{cav}}/m$, where m is an integer, for varying nuclear radii R_1 and RIs n_1. Finally, the transverse modes were computed using a numerical mode solver as shown by the solid lines in Fig. 4. For reference, the wavelength shift calculated only on the axis of the cell while neglecting transverse mode confinement, referred to as the one-dimensional (1-D) model, is shown in dashed lines. Comparison of the two sets of curves highlights that transverse mode confinement effects are important for correctly interpreting mode shifts.

The relationship between nuclear RI and size modeled for the experimentally observed nuclear mode shift of 24.59 nm is shown in Fig. 5. The double sphere model offers an improved estimate of nuclear RI, especially for cells with a small nucleus. A nuclear size resolution of 0.02 μm for optofluidic intracavity spectroscopy can be estimated based on a wavelength shift of 10% of the 0.5-nm linewidth, and compares favorably with the 3% or $\sim$1 μm resolution of conventional flow cytometry.

V. Conclusion

This letter reports the spectroscopic properties of canine lymphoma and lymphocytes within optofluidic microcavities fabricated in glass. The distinctive spectral properties of cancerous cells relative to normal ones can be directly used for quick cancer detection without further RI calculations from the spectra in contrast to work based on longitudinal mode shifts. If RIs are to be calculated, especially for cells with a small nucleus, lateral confinement effects should be considered as indicated by the double sphere effective index model.

Acknowledgment

The authors would like to thank B. Rose and A. A. Cunkelman at the CSU veterinary hospital for assistance in cell culturing.

References

[1] J. Beuthan, O. Minet, J. Helfmann, M. Herrig, and G. Muller, "The spatial variation of the refractive index in biological cells," *Phys. Med. Biol.*, vol. 41, no. 3, pp. 369–382, Mar. 1996.

[2] V. Backman, M. B. Wallace, and L. T. Arendt *et al.*, "Detection of preinvasive cancer cells," *Nature*, vol. 406, no. 6791, pp. 35–36, Jul. 2000.

[3] R. A. Flynn, B. Shao, M. Chachisvilis, M. Ozkan, and S. C. Esener, "Two-beam optical traps: Refractive index and size measurements of microscale objects," *Biomed. Microdevices*, vol. 7, no. 2, pp. 93–193, 2005.

[4] S. Piper, *private communication.* Feb. 2007.

[5] D. Kumar, H. Shao, and K. L. Lear, "Microfluidic cavity surface emitting laser based biosensor," in *2004 IEEE LEOS Annu. Meeting Conf. Proc.*, Rio Grande, Puerto Rico, 2004, vol. 1, pp. 118–119.

[6] H. Shao, D. Kumar, and K. L. Lear, "Single-Cell detection using optofluidic intracavity spectroscopy," *IEEE Sensors J.*, vol. 6, no. 6, pp. 1543–1550, Dec. 2006.

[7] W. Z. Song, X. M. Zhang, A. Q. Liu, and C. S. Lim, "Refractive index measurement of single living cells using on-chip Fabry–Pérot cavity," *Appl. Phys. Lett.*, vol. 89, pp. 203901-1–203901-2, 2006.

[8] P. L. Gourley, "Biocavity laser for high-speed cell and tumour biology," *J. Phys. D, Appl. Phys.*, vol. 36, no. 14, pp. R228–R239, Jul. 21, 2003.

[9] H. Shao, D. Kumar, S. A. Feld, and K. L. Lear, "Fabrication of a Fabry–Pérot cavity in a microfluidic channel using thermocompressive gold bonding of glass substrates," *IEEE J. MEMS*, vol. 15, no. 4, pp. 756–762, Aug. 2005.

[10] A. N. Shvalov, I. V. Surovtsev, A. V. Chenyshev, J. T. Soini, and V. P. Maltsev, "Paticle classification from sctaterring with the scanning flow cytometer," *Cytometry A*, vol. 37, no. 3, pp. 215–220, 1999.

[11] K. W. Keohane and W. K. Metcalf, "The cytoplasmic refractive index of lymphocytes, its significance and its changes during active immunization," *Q J. Exp. Physiol. Cogn. Med. Sci.*, vol. 44, pp. 343–350, 1959.

[12] P. M. A. Sloot, A. G. Hoekstra, and C. G. Figdor, "Osmotic response of lymphocytes measured by means of forward light scattering: Theoretical considerations," *Cytometry A*, vol. 9636, pp. 636–641, 1988.

[13] C. Liu and C. E. Capjack, "Effects of cellular fine structure on scattered light pattern," *IEEE Trans. Nanobiosci.*, vol. 5, no. 2, pp. 76–82, Jun. 2006.

[14] G. R. Hadley, Opt. Lett. "Effective index model for vertical-cavity surface-emitting lasers," 1995, vol. 20, no. 13, pp. 1483–1485.

[15] C. Williams, *Cancer Biology and Management: An Introduction.* West Sussex, England: Wiley, 1990.